AMRX Applied Mathematics Research eXpress
Volume 2006, Article ID 15487, Pages 1–21

Growing Surfactant Waves in Thin Liquid Films Driven by Gravity

Thomas P. Witelski, Michael Shearer, and Rachel Levy

The dynamics of a gravity-driven thin film flow with insoluble surfactant are described in the lubrication approximation by a coupled system of nonlinear PDEs. When the total quantity of surfactant is fixed, a traveling wave solution exists. For the case of constant flux of surfactant from an upstream reservoir, global traveling waves no longer exist as the surfactant accumulates at the leading edge of the thin film profile. The dynamics can be described using matched asymptotic expansions for $t \to \infty$. The solution is constructed from quasistatically evolving traveling waves. The rate of growth of the surfactant profile is shown to be $O(\sqrt{t})$ and is supported by numerical simulations.

1 Introduction

The dynamics of thin liquid films on solid substrates have been studied extensively in a variety of contexts, including gravity-driven flows [4, 12, 22, 31], spin-coating [30], and flows driven by strong surface tension [1, 25, 26]. Under lubrication theory, the governing equations for free-surface Stokes flow of thin films of viscous fluids can be reduced to a single nonlinear evolution equation for the surface height, $h = h(x,t)$ [26]. When surface tension is significant, the equation is fourth-order. *Marangoni surface stresses* are driving forces created by variations in the coefficient of surface tension. These forces can be generated by thermal [2, 23], electrical [19], or chemical means [20]. Flows driven by Marangoni stresses have been found to yield interesting instabilities and new kinds

Received 30 June 2006; Revised 11 October 2006; Accepted 30 October 2006

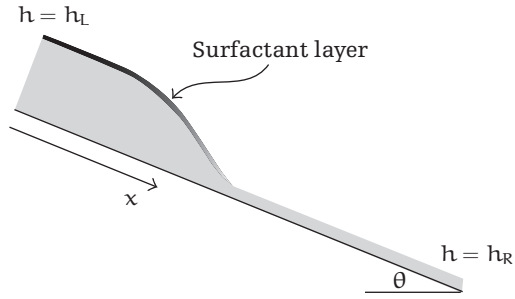

Figure 1.1 Schematic representation of a monolayer of insoluble surfactant (with local concentration Γ indicated by grayscale shading) spreading on a thin film with local height h (tan region) flowing down an inclined plane.

of waves [2, 5, 14, 21]. Chemical Marangoni stresses can be generated by the presence of *surfactants* (surface active agents), which typically decrease surface tension; nonuniform distributions of surfactant molecules creates such surface stresses [3, 13, 14]. Insoluble surfactants are transported by the fluid flow at the free surface, leading to a coupled PDE system for the concentration of surfactant and the film height [3, 9, 27–29] (see Figure 1.1).

In a series of recent numerical studies, Edmonstone, Matar, and Craster [6, 7] considered one-dimensional flow with surfactant down an inclined plane, and explored the stability to transverse perturbations. An interesting observation arising from their study is that when surfactant is supplied from an upstream reservoir, it accumulates at the leading edge of the flow, resulting in a steady increase of the maximum surfactant concentration (see Figure 1.2). Motivated by these observations, we present an analysis of this problem that determines the evolution of the surfactant profile. Our work builds on the results of [16, 17] to explain the structure of solutions in terms of traveling waves of a simplified problem in which capillarity and other regularizing influences are neglected. One result emerging from these studies is that the flow on an inclined plane is significantly different from the spreading of fluid on a horizontal surface [13, 14, 20, 27–29].

Model equations. Let $h = h(x,t) \geq 0$ be the nondimensional height of the free surface of the fluid film, and let $\Gamma = \Gamma(x,t) \geq 0$ denote the scaled concentration of insoluble surfactant on the free surface, where x is the position measured down the inclined plane. The

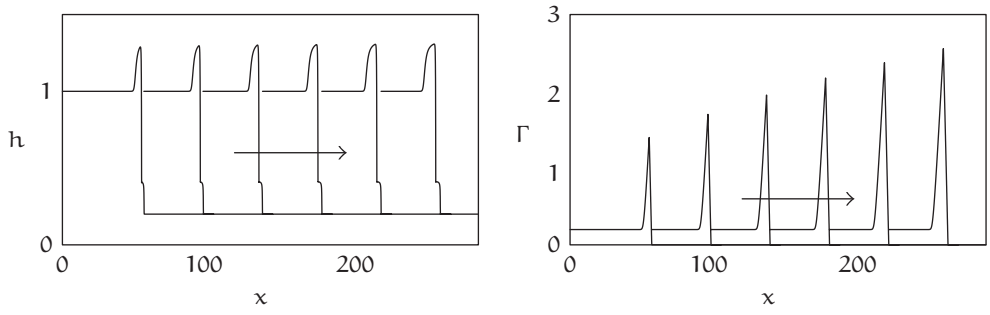

(a) (b)

Figure 1.2 Evolution of the film thickness $h(x,t)$ (a) and the surfactant concentration $\Gamma(x,t)$ (b) from numerical simulations of system (1.1a) and (1.1b) with a steady influx of supply of surfactant at $x = 0$ with $\Gamma_L > 0$.

system of governing equations is [6, 7, 16, 17, 27]

$$h_t + \left(\frac{1}{3}h^3\right)_x - \left(\frac{1}{2}h^2\Gamma_x\right)_x = \beta\left(\frac{1}{3}h^3h_x\right)_x, \tag{1.1a}$$

$$\Gamma_t + \left(\frac{1}{2}h^2\Gamma\right)_x - \left(h\Gamma\,\Gamma_x\right)_x = \beta\left(\frac{1}{2}h^2\Gamma\,h_x\right)_x + \delta\Gamma_{xx}. \tag{1.1b}$$

We consider this system on the half line $x \geq 0$ with boundary conditions

$$h(0,t) = h_L, \quad h(x \longrightarrow \infty, t) = h_R, \tag{1.2a}$$

$$\Gamma(0,t) = \Gamma_L, \quad \Gamma(x \longrightarrow \infty, t) = 0. \tag{1.2b}$$

The terms with coefficients β, δ on the right-hand side regularize the underlying transport equations. In this model, we have omitted fourth-order regularizing capillarity terms. The role of these terms will be shown to have a weak influence on the wave structures studied here, as will be described in a forthcoming paper [17].

We restrict attention to the case $h_L > h_R$ in which an advancing front moves down the inclined plane, into a precursor film with height h_R. The precursor film will typically be very thin compared to the upstream film, that is, $h_L \gg h_R$. The problem statement is completed by specifying initial conditions

$$h(x,0) = h_*(x) \geq h_R, \qquad \Gamma(x,0) = \Gamma_*(x) \geq 0. \tag{1.3}$$

Integrating (1.1b) over the domain yields the rate of growth of the total surfactant mass, I, in terms of the flux set by the boundary conditions at $x = 0$,

$$\frac{dI}{dt} = \frac{d}{dt}\left(\int_0^\infty \Gamma(x,t)dx\right) = \frac{1}{2}h_L^2\Gamma_L. \tag{1.4}$$

If $\Gamma_L = 0$, then the mass of surfactant is conserved for all times, that is, $dI/dt = 0$; this is sometimes called the constant volume (of surfactant) case [6, 7]. For constant $\Gamma_L > 0$ the mass of surfactant grows linearly in time, that is, $I(t) = (1/2)h_L^2\Gamma_L(t + t_*)$, where the constant t_* is related to the mass of the initial data. The boundary condition can be interpreted as describing a reservoir with an unlimited supply of surfactant which maintains the constant surfactant concentration Γ_L at $x = 0$ (see Figure 1.2).

For $\beta = \delta = 0$ (1.1a) and (1.1b) form a coupled hyperbolic-degenerate parabolic system [28] that sustains wave-like solutions with finite propagation speed. While sharing elements with models for wave propagation in hyperbolic conservation laws and traveling waves in parabolic equations [10, 18, 32] such thin-film/surfactant systems have novel features that make them the focus of continuing mathematical analysis [3, 9, 17, 27–29].

In this article, we focus on the influence of the surfactant boundary condition parameter $\Gamma_L \geq 0$; the results and analysis depend on an understanding of the special case $\Gamma_L = 0$, in which the total mass of surfactant in the system is fixed. In Section 2, we review and generalize the weak traveling wave solution found in [16] for $\Gamma_L = 0$. In Section 3, a quasistatically growing traveling wave is constructed via matched asymptotics; it describes the dynamics for $\Gamma_L > 0$. In particular, a simple $O(\sqrt{t})$ self-similar growth of the long-time surfactant distribution is predicted by asymptotics, and verified by results from numerical simulations of (1.1a) and (1.1b).

2 Traveling waves for $\Gamma_L = 0$ with $\beta = \delta = 0$

In the absence of regularization (i.e., $\beta = \delta = 0$) system, (1.1a), and (1.1b) have traveling wave solutions, as described by [16]. Here we summarize the analysis from [16], as it provides the starting point for our study of the current problem.

Consider steady profile traveling wave solutions with speed s,

$$h(x,t) = \overline{h}(\eta), \quad \Gamma(x,t) = \overline{\Gamma}(\eta), \quad \eta = x - st. \tag{2.1}$$

Substituting (2.1) into (1.1a) and (1.1b) and integrating the resulting system of ODEs once in η yields

$$-s\overline{h}+\frac{1}{3}\overline{h}^3-\frac{1}{2}\overline{h}^2\frac{d\overline{\Gamma}}{d\eta}=\frac{1}{3}\beta\overline{h}^3\frac{d\overline{h}}{d\eta}-k_h, \tag{2.2a}$$

$$-s\overline{\Gamma}+\frac{1}{2}\overline{h}^2\overline{\Gamma}-\overline{h}\,\overline{\Gamma}\frac{d\overline{\Gamma}}{d\eta}=\frac{1}{2}\beta\overline{h}^2\overline{\Gamma}\frac{d\overline{h}}{d\eta}+\delta\frac{d\overline{\Gamma}}{d\eta}-k_\Gamma, \tag{2.2b}$$

where k_h, k_Γ are constants of integration. Imposing the asymptotic boundary conditions $\overline{h}(\eta\to-\infty)\to h_L$ and $\overline{h}(\eta\to\infty)\to h_R$ in (2.2a) with the assumption that $\overline{h}', \overline{\Gamma}'\to 0$ for $|\eta|\to\infty$, we find

$$s=\frac{1}{3}\left(h_L^2+h_Lh_R+h_R^2\right)>0, \qquad k_h=\frac{1}{3}h_Lh_R\left(h_L+h_R\right)>0. \tag{2.3}$$

Furthermore, if the surfactant profile satisfies $\overline{\Gamma}(\eta\to\pm\infty)=0$ then (2.2b) forces $k_\Gamma=0$.

For $\beta=\delta=0$, the solution is a weak solution of (2.2a) and (2.2b) in which $\overline{h}(\eta)$ and $\overline{\Gamma}'(\eta)$ are piecewise constant (see Figure 2.1) [16]:

$$\overline{h}(\eta)=\begin{cases}h_L, & \eta<\eta_1,\\ h_1, & \eta_1<\eta<0,\\ h_2, & 0<\eta<\eta_2,\\ h_R, & \eta_2<\eta,\end{cases} \qquad \overline{\Gamma}'(\eta)=\begin{cases}0, & \eta<\eta_1\\ G_1, & \eta_1<\eta<0,\\ G_2, & 0<\eta<\eta_2,\\ 0, & \eta_2<\eta.\end{cases} \tag{2.4}$$

The values of the four constants $\{h_j, G_j\}$ for $j=1,2$ in (2.4) are determined by satisfying coupled algebraic jump conditions at $\eta=0,\eta_1,\eta_2$. In [16, 17] it is shown that the values h_1, h_2 satisfying $0\le h_R<h_2<h_L<h_1$ are given by the positive real roots of the polynomial equation

$$h^3-6sh+12k_h=0. \tag{2.5}$$

These roots exist if and only if the ratio of downstream to upstream film heights is below a threshold:

$$0\le\frac{h_R}{h_L}<\frac{1}{2}\left(\sqrt{3}-1\right). \tag{2.6}$$

The surfactant slopes $G_1>0$, $G_2<0$ are then given by

$$G_1=\frac{\left(h_1-h_2\right)\left(2h_1+h_2\right)}{6h_1}, \qquad G_2=-\frac{\left(h_1-h_2\right)\left(h_1+2h_2\right)}{6h_2}. \tag{2.7}$$

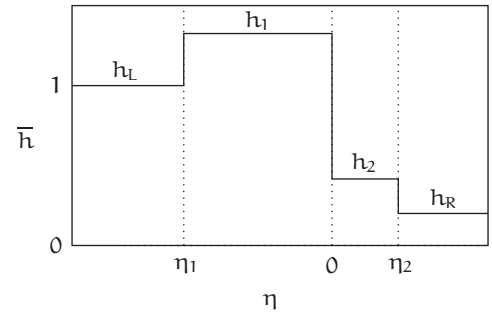

(a)

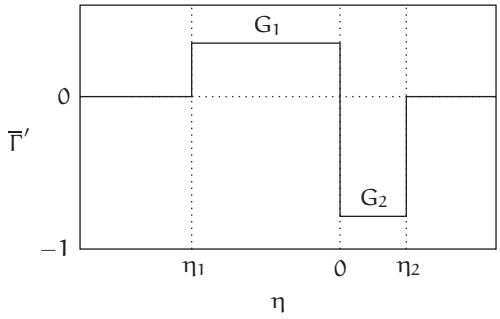

(b)

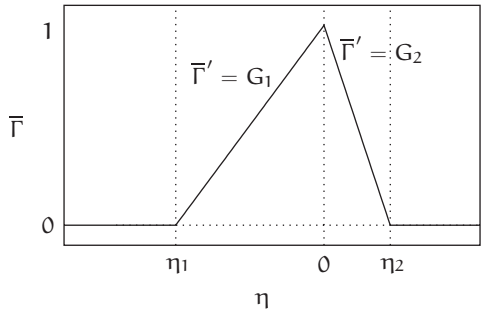

(c)

Figure 2.1 The weak traveling solution (2.4): (a) the piecewise constant $\overline{h}(\eta)$ profile, (b) the piecewise constant $\overline{\Gamma}'(\eta)$ profile, and (c) the piecewise linear profile for $\overline{\Gamma}(\eta)$ (2.8). For imposed boundary conditions $h_L = 1$ and $h_R = 0.1$, (2.5), (2.7), and (2.9) yield the values $h_1 \approx 1.3787$, $h_2 \approx 0.2019$, $G_1 \approx 0.4210$, $G_2 \approx -1.7316$, $\eta_1 \approx -2.3753$, $\eta_2 \approx 0.5775$.

The surfactant profile is continuous and piecewise linear [16], consequently, integrating the solution for $\overline{\Gamma}'(\eta)$ subject to the condition $\overline{\Gamma}(0) = 1$ yields the solution

$$\overline{\Gamma}(\eta) = \begin{cases} 0, & \eta \le \eta_1, \\ 1 + G_1\eta, & \eta_1 \le \eta \le 0, \\ 1 + G_2\eta, & 0 \le \eta \le \eta_2, \\ 0, & \eta_2 \le \eta, \end{cases} \tag{2.8}$$

where continuity of $\overline{\Gamma}(\eta)$ at $\overline{\Gamma} = 0$ determines the values η_1, η_2 to be

$$\eta_1 = -\frac{1}{G_1} < 0, \qquad \eta_2 = -\frac{1}{G_2} > 0. \tag{2.9}$$

Observe that the surfactant distribution is compactly supported and has total mass

$$\overline{I} = \int_{-\infty}^{\infty} \overline{\Gamma} d\eta = \frac{1}{2}(\eta_2 - \eta_1) = \frac{6(h_1 + h_2)}{(h_1 + 2h_2)(2h_1 + h_2)}. \tag{2.10}$$

From the geometry of Figure 2.1(c), $\overline{I}$ is the area of the triangular profile $\overline{\Gamma}(\eta)$.

Remarks 2.1. (1) In the forthcoming article [17], it will be shown that this solution is structurally stable with respect to regularizations introduced by diffusive transport of surfactant ($\delta > 0$), diffusive transport of bulk fluid due to gravitational body forces ($\beta > 0$), and capillarity (the effects of surface tension). These regularizations are shown to leave h_1, h_2 and G_1, G_2 essentially unchanged; their effects are localized to the neighborhoods of the points $\eta = 0, \eta_1, \eta_2$.

(2) If the precursor thickness h_R approaches zero, we find (from [17]) that $h_2 \to 0$ and $h_1 \to \sqrt{2}h_L$. Consequently, from (2.7), $G_2 \to -\infty$ (a shock in the surfactant profile at $\eta = 0$) while G_1 remains finite. From (2.9), $\eta_2 \to 0$; and hence the h_2 plateau in the film thickness vanishes, while the surfactant profile approaches a sawtooth wave.

2.1 Scale-invariant structure of the traveling wave

The condition $\overline{\Gamma}(0) = 1$ determining the maximum surfactant concentration is an arbitrary normalization. This condition can be imposed at $\eta = 0$ thanks to translation invariance of the PDEs (1.1a) and (1.1b). The maximum value itself can be set to any positive constant, $\Gamma_{max} \equiv m > 0$. In [16] it was noted that the solutions of (1.1a) and (1.1b) with

$\beta = \delta = 0$ are invariant under the continuous one-parameter scaling $h \to h$, $\Gamma \to m\Gamma$, $x \to x/m$, $t \to t/m$. Consequently, up to translation invariance, the general traveling wave solution of (1.1a) and (1.1b) with $\beta = \delta = 0$ subject to boundary conditions (1.2a) and (1.2b) with $\Gamma_L = 0$ is

$$h(x,t) = \overline{h}\left(\frac{x-st}{m}\right), \qquad \Gamma(x,t) = m\overline{\Gamma}\left(\frac{x-st}{m}\right) \tag{2.11}$$

for any $m > 0$.

Note that the trivial case of no surfactant ($\Gamma \equiv 0$) corresponds to the singular case of (2.11) with $m = 0$,

$$\overline{h}_0(\eta) = \begin{cases} h_L, & \eta < 0, \\ h_R, & 0 < \eta, \end{cases} \qquad \overline{\Gamma}_0(\eta) \equiv 0. \tag{2.12}$$

The wave speed given by (2.3) is independent of $m \geq 0$. For $m = 0$, this is to be expected from the fact that (2.12) is the shock wave solution of the decoupled equation $h_t + ((1/3)h^3)_x = 0$, a scalar conservation law. We can therefore interpret the influence of the surfactant as modifying the shape of the surfactant-free shock profile (2.12), effectively broadening the width of the shock structure through the introduction of the h_1 and h_2 plateau regions. In the limit of vanishing surfactant concentration, $\Gamma_{max} \to 0$, we observe that $\eta_2 - \eta_1 \to 0$, so although h_1, h_2 are independent of Γ_{max}, solution (2.11) collapses to solution (2.12), shrinking the plateau with height h_1 to zero width.

It is noteworthy that solution (2.11) depends upon having upstream and downstream film heights below the critical ratio (2.6). If $(1/2)(\sqrt{3}-1) < h_R/h_L < 1$, then a different solution emerges from PDE simulations, even though the surfactant-free solution is still a single monotonic traveling wave. The structure of the new solution is the subject of current investigation.

3 Dynamics for $\Gamma_L > 0$ with $\beta, \delta > 0$

We now focus on understanding the role of the boundary condition parameter Γ_L in determining the dynamics, as in the simulation with $\Gamma_L > 0$ shown in Figure 1.2.

If $\Gamma_L = 0$, then the total amount of surfactant is conserved for all times. If $\beta = \delta = 0$ and we have a traveling wave solution (2.11) for the surfactant profile, then the value of m is determined by the mass of the initial condition $\Gamma_*(x)$ (1.3),

$$I = \int_0^\infty \Gamma_*(x)dx = m^2 \int \overline{\Gamma}(\zeta)d\zeta = m^2\overline{I} \tag{3.1}$$

with $\bar{\Gamma}$ given by (2.10). More generally, we expect that the traveling wave solution (2.11) is structurally stable and attracting for $t \to \infty$ from a broader set of initial data and small positive β, δ.

If $\Gamma_L > 0$, then there are no smooth bounded traveling wave solutions of (2.2a) and (2.2b) satisfying upstream and downstream boundary conditions. To see this, we note that the upstream condition implies $k_\Gamma = ((1/2)h_L^2 - s)\Gamma_L$, whereas the downstream boundary condition gives $k_\Gamma = 0$. For $\Gamma_L > 0$ these are consistent only in the special case $s = (1/2)h_L^2$; from (2.3), this yields the condition $h_R/h_L = (1/2)(\sqrt{3} - 1)$, the threshold value from (2.6). This leads to the trivial solution $h = \textit{constant}$ as the only bounded traveling wave at this speed. But this solution conflicts with the boundary conditions, $h_L > h_R$, so it is not acceptable. Consequently, the solution of (1.1a) and (1.1b) in this case must take a different form; we will turn to the use of matched asymptotics to construct the solution.

The behavior observed in numerical simulations in Figure 1.2 suggests that the solution with $\Gamma_L > 0$ still resembles the traveling wave solution (2.11). However, the Γ profile evolves, suggesting that the maximum of Γ should be generalized to be a time-dependent increasing function, $m(t)$, to be used in (2.11). We now present analysis to support this description.

3.1 Approximate global solution for $t \to \infty$

Motivated by the above discussion, we consider a change of variables that allows for time-dependence in the maximum of Γ and in the speed of propagation. All solutions of (1.1a) and (1.1b) can be written in the form

$$h(x,t) = \widetilde{h}(\zeta,t), \quad \Gamma(x,t) = m(t)\widetilde{\Gamma}(\zeta,t), \quad \zeta = \frac{x - x_0(t)}{m(t)}, \tag{3.2}$$

where the functions $x_0(t)$, $m(t)$ must be determined. Substituting (3.2) into (1.1a) and (1.1b) yields the new governing PDEs:

$$\widetilde{h}_t - x_0'(t)\widetilde{h}_\zeta - m'(t)\zeta\widetilde{h}_\zeta + \left(\frac{1}{3}\widetilde{h}^3\right)_\zeta - \left(\frac{1}{2}\widetilde{h}^2\widetilde{\Gamma}_\zeta\right)_\zeta = \frac{\beta}{m(t)}\left(\frac{1}{3}\widetilde{h}^3\widetilde{h}_\zeta\right)_\zeta, \tag{3.3a}$$

$$\widetilde{\Gamma}_t - x_0'(t)\widetilde{\Gamma}_\zeta - m'(t)\zeta\widetilde{\Gamma}_\zeta + m'(t)\widetilde{\Gamma} + \left(\frac{1}{2}\widetilde{h}^2\widetilde{\Gamma}\right)_\zeta - \left(\widetilde{h}\widetilde{\Gamma}\widetilde{\Gamma}_\zeta\right)_\zeta = \frac{\beta}{m(t)}\left(\frac{1}{2}\widetilde{h}^2\widetilde{\Gamma}\widetilde{h}_\zeta\right)_\zeta + \frac{\delta}{m(t)}\widetilde{\Gamma}_{\zeta\zeta}. \tag{3.3b}$$

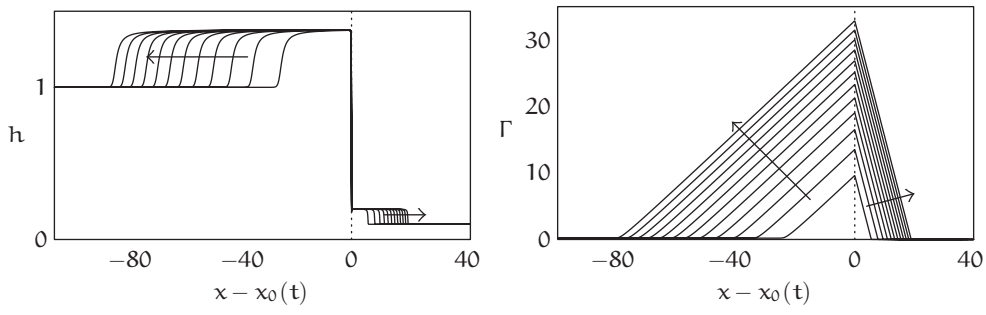

(a) (b)

Figure 3.1 Long-time evolution of the film thickness $h(x,t)$ (a) and the surfactant concentration $\Gamma(x,t)$ (b) from numerical simulations of system (1.1a) and (1.1b) with $h_L = 1$, $h_R = 0.1$, $\beta = 0.1$, $\delta = 0.01$, and $\Gamma_L = 0.2$. Time profiles for $t = 5000, 10000, 15000, \ldots, 60000$ shifted into the reference frame $x - x_0(t)$ where the position of the maximum of $\Gamma(x,t)$ is stationary.

For concreteness, in numerical simulations, $x_0(t)$ will be defined by the position of the maximum of $\Gamma(x,t)$. Figure 3.1 shows that in this moving reference frame, h, Γ exhibit a well-defined growth. To depict the scaled forms $\widetilde{h}$ and $\widetilde{\Gamma}$, the same profiles are plotted in the forms (3.2) in Figure 3.2 with $m(t)$ replaced by the numerical result $\Gamma_{max}(t) = \max_x \Gamma(x,t)$.

Plotted in this form, the profiles indeed appear to approach the traveling wave solution, (2.4) and (2.8), as $t \to \infty$. This behavior can be obtained directly from (3.3a) and (3.3b) subject to the following assumptions.

(1) As $t \to \infty$, the rescaled solutions $\widetilde{h}$, $\widetilde{\Gamma}$ converge to quasisteady profiles that are independent of t: $\widetilde{h} \to \widetilde{h}(\zeta)$, $\widetilde{\Gamma} \to \widetilde{\Gamma}(\zeta)$.

(2) The maximum of the surfactant profile grows slowly (sublinearly) with time,

$$m(t) = O\left(t^{\alpha}\right), \quad \text{as } t \longrightarrow \infty \text{ with } 0 < \alpha < 1. \tag{3.4}$$

(3) The propagation speed $x_0'(t)$ remains bounded for all times and approaches a positive constant: $x_0'(t) \to \widetilde{s} > 0$, as $t \to \infty$.

Assumption (1), supported by Figure 3.2, suggests that the $\widetilde{h}_t$, $\widetilde{\Gamma}_t$ terms in (3.3a) and (3.3b) can be neglected to yield equations involving only ζ-derivatives of $\widetilde{h}$, $\widetilde{\Gamma}$. From assumption (2), $m(t) \to \infty$ and $m'(t) \to 0$ as $t \to \infty$. Consequently, the terms on the

right-hand sides of (3.3a) and (3.3b) will vanish since $\beta/m \to 0$ and $\delta/m \to 0$. Thus regularization offered by these terms becomes negligible for long times. Similarly, the terms on the left-hand sides multiplied by $m'(t)$ become negligible (with the mild assumption that $\zeta\widetilde{h}_\zeta$, $\zeta\widetilde{\Gamma}_\zeta$ are bounded as $|\zeta| \to \infty$). Using assumption (3), the resulting equations for $t \to \infty$ can be integrated once in ζ to yield

$$-\widetilde{s}\widetilde{h} + \frac{1}{3}\widetilde{h}^3 - \frac{1}{2}\widetilde{h}^2\frac{d\widetilde{\Gamma}}{d\zeta} = -k_{\widetilde{h}}, \tag{3.5a}$$

$$-\widetilde{s}\widetilde{\Gamma} + \frac{1}{2}\widetilde{h}^2\widetilde{\Gamma} - \widetilde{h}\widetilde{\Gamma}\frac{d\widetilde{\Gamma}}{d\zeta} = -k_{\widetilde{\Gamma}}, \tag{3.5b}$$

where $k_{\widetilde{h}}$, $k_{\widetilde{\Gamma}}$ are constants of integration. Suitable boundary conditions corresponding to (1.2a), (1.2b) are given by

$$\widetilde{h}(\zeta \longrightarrow -\infty) = h_L, \qquad \widetilde{h}(\zeta \longrightarrow \infty) = h_R, \tag{3.5c}$$

$$\widetilde{\Gamma}(\zeta \longrightarrow -\infty) = 0, \qquad \widetilde{\Gamma}(\zeta \longrightarrow \infty) = 0. \tag{3.5d}$$

The boundary condition on $\widetilde{\Gamma}(\zeta \to -\infty)$ follows from $\widetilde{\Gamma}(\zeta \to \infty) = \Gamma_L/m(t) \to 0$ as $t \to \infty$. As a result, the influence of the boundary condition Γ_L does not enter in the leading order problem (3.5a) and (3.5b) for $t \to \infty$. At this point, we observe that problem (3.5a) and (3.5b) reduces to that of Section 2 (2.2a) and (2.2b) and we have the leading order solution for $t \to \infty$,

$$\widetilde{h}(\zeta, t) \sim \overline{h}(\zeta), \qquad \widetilde{\Gamma}(\zeta, t) \sim \overline{\Gamma}(\zeta), \qquad x_0'(t) \sim s. \tag{3.6}$$

Returning to the original PDE system (1.1a) and (1.1b) on the domain $x > 0$, assumption (2) is justified by considering the evolution of the mass of surfactant. Figure 1.2 suggests that the surfactant profile with $\Gamma_L > 0$ can be approximated by a uniform layer with $\Gamma = \Gamma_L$ together with a growing triangular profile (2.8), scaled as in (2.11) by $m(t)$. With respect to calculating the mass of surfactant, this approximate description of $\Gamma(x, t)$ can be expected to yield a vanishingly small relative error as $t \to \infty$. Hence for long times, $I(t)$ is given by

$$I(t) = \int_0^\infty \Gamma dx \approx \Gamma_L s\big(t + t_0\big) + \frac{1}{2}\Gamma_L^2\big|\eta_1\big| + m^2(t)\int_{\eta_1}^{\eta_2} \overline{\Gamma}(\eta)d\eta, \tag{3.7}$$

where t_0 is a constant related to initial conditions. The first term on the right of (3.7) is the surfactant in the uniform Γ_L layer with length increasing at a rate equal to the

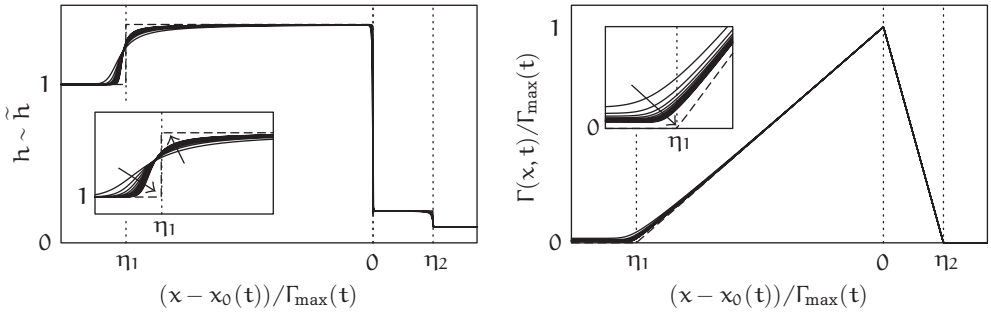

(a) (b)

Figure 3.2 The long-time solution profiles from Figure 3.1 rescaled according to (3.2). Dashed lines show the traveling wave solution (2.4), (2.8). Insets show details of the evolution near $\eta_1 \approx -2.375$, given by (2.9).

propagation speed of the advancing triangular wave (asymptotically $x_0' \sim s$). The second term is a finite contribution from the region joining the uniform layer to the triangular profile. Substituting (3.7) into (1.4) yields

$$\frac{dI}{dt} \approx \bar{I}\frac{d(m^2)}{dt} + s\Gamma_L = \frac{1}{2}h_L^2\Gamma_L. \tag{3.8}$$

Using (2.3), we obtain

$$m(t) \sim \left(\frac{\Gamma_L}{6\bar{I}}\left(h_L^2 - 2h_Lh_R - 2h_R^2\right)\right)^{1/2}\sqrt{t+t_*}, \quad t \longrightarrow \infty. \tag{3.9}$$

Consequently, the second assumption, (3.4), is verified with $\alpha = 1/2$.[1] Observe that the condition that the coefficient of (3.9) be real requires that $1 - 2r - 2r^2 > 0$, where r is the ratio $r = h_R/h_L$. The resulting condition on this ratio is $0 < r < (1/2)(\sqrt{3}-1)$, precisely coinciding with the condition (2.6) for the existence of steady profile waves [16]. Figure 3.3 shows excellent agreement between the prediction (3.9) and the results of the numerical simulations.

[1]Note that the traveling wave solution (3.6) could also be expected for time-dependent boundary conditions, $\Gamma_L(t) = O(t^\gamma)$ if $0 \le \gamma < 1$. For $\gamma = 1$, the $m'(t)$ terms on the left-hand sides of (3.3a) and (3.3b) must be retained, which would lead to a new class of self-similar solutions.

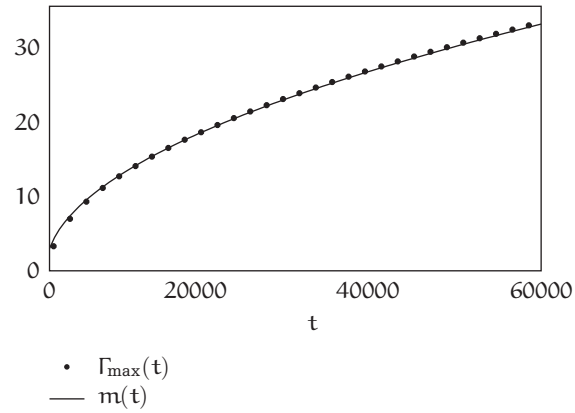

Figure 3.3 Comparison of the maximum surfactant concentration from the numerical simulation of Figures 3.1, 3.2, $\Gamma_{max}(t) = \max_x \Gamma(x,t)$ (solid dots) and the predicted evolution $m(t)$ given by (3.9) (solid curve).

In summary, we have shown that for long times, the solutions approach growing traveling waves,

$$h(x,t) \sim \overline{h}\left(\frac{x - x_0(t)}{m(t)}\right), \qquad \Gamma(x,t) \sim m(t)\overline{\Gamma}\left(\frac{x - x_0(t)}{m(t)}\right). \tag{3.10}$$

Some further comments are appropriate at this point. First, for large times, when the influence of the boundary conditions at $x = 0$ are weak, the traveling wave solutions of (1.1a) and (1.1b) should be invariant with respect to spatial translations, $x \to x + \epsilon_1$ for any real ϵ_1. But secondly, from the autonomous equations (3.5a) and (3.5b), the long time growing solutions (3.2) should also be invariant with respect to translations in their spatial variable, $\zeta \to \zeta + \epsilon_2$ for some ϵ_2. Combining these observations, we note that the general form for the moving reference frame for $t \to \infty$ is

$$x_0(t) \sim st - \epsilon_2 m(t) - \epsilon_1 \Longrightarrow \frac{dx_0}{dt} \sim s - \epsilon_2 m'(t) \sim s. \tag{3.11}$$

This validates the third assumption. See Figure 3.4(a) for numerical evidence supporting (3.11). If $x_0(t)$ is known, then from (3.2) the positions defining the region of support of the dominant distribution (η_1, η_2) are given by

$$x_1(t) = x_0(t) + \eta_1 m(t), \qquad x_2(t) = x_0(t) + \eta_2 m(t), \tag{3.12}$$

see Figure 3.4(b).

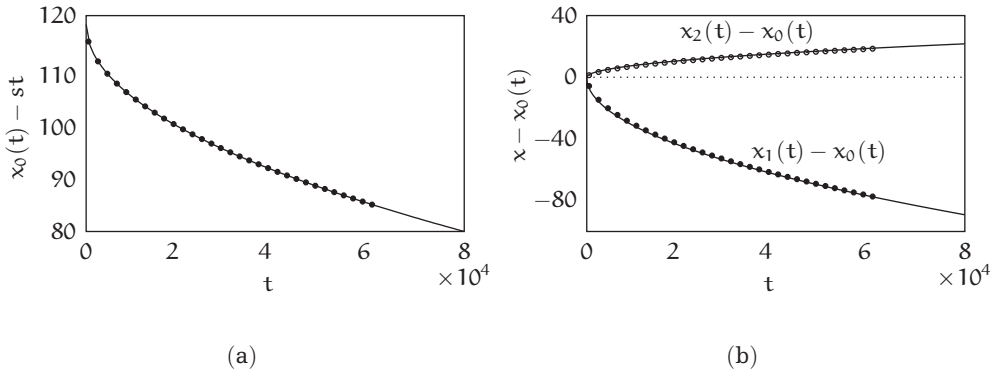

Figure 3.4 (a) Position of the moving reference frame relative to the asymptotic traveling wave speed $s = 0.37$ from (2.3), values from the numerical simulation (solid dots) show a $O(c_1 + c_2\sqrt{t})$ lag (solid curve) as predicted by (3.11). (b) Positions of the edges of the region of support of the triangular surfactant profile relative to $x_0(t)$, numerical simulation values (dots) compared with prediction (3.12) (solid curves) with $\eta_1 \approx -2.375$, $\eta_2 \approx 0.5775$, given by (2.9), and $m(t) \approx 0.1327\sqrt{t + t_*}$ from (3.9) for $h_L = 1$, $h_R = 0.1$ and $\Gamma_L = 0.2$.

One final remaining issue is that while (3.10) suggests that $\Gamma(x,t) = 0$ for $x < x_1(t)$, it is clear from Figure 1.2 that $\Gamma \sim \Gamma_L > 0$. This is resolved in the next subsection via boundary layer analysis.

3.2 Boundary layer structures at the jump discontinuities η_1 and η_2

The limit $1/m \to 0$ in (3.3a) and (3.3b) eliminated the regularization given by the second-order terms on the right-hand sides of those equations. This is a singular perturbation [11, 15] of the full system for $t \to \infty$; and hence the weak solution (3.10) should be interpreted as a leading order *outer solution*. In particular, it is not uniformly valid for all ζ; at points where jump discontinuities occur in $\overline{h}(\zeta), \overline{\Gamma}(\zeta)$, the influence of the higher-order terms may strongly influence the local structure of the solution, see insets in Figure 3.2. In this section, we use matched asymptotics to construct boundary layer solutions as inner expansions of the solution in the neighborhoods of the shocks at η_1 and η_2. These inner solutions can be combined with (3.10) and a boundary layer at $\eta = 0$ (considered in Section 3.3) to yield a uniformly valid approximate solution.

Define $\epsilon \equiv 1/m \to 0$ as a small parameter for the limit $t \to \infty$. Consider a small neighborhood of the shock at $\zeta = \eta_1$, defined by $\zeta = \eta_1 + \epsilon^\lambda y$ with $\lambda > 0$ to be determined and $y = O(1)$. The profile $\widetilde{h}$ remains finite and bounded, so the quasisteady solution

should take the form $\widetilde{h} = \widehat{h}(y) + O(\epsilon)$. Similarly, we expect that for $\zeta \leq \eta_1$ the scaled surfactant is of the order $\widetilde{\Gamma} \approx \Gamma_L/m = O(\epsilon)$, hence the solution should be $\widetilde{\Gamma} = \epsilon\widehat{\Gamma}(y) + O(\epsilon^2)$. Substituting these into (3.3a) and (3.3b) and balancing the dominant terms determines the scaling to be $\lambda = 1$ and (after integrating in y) yields the leading order equations:

$$-\left[\widehat{s}_1 + \eta_1 m'(t)\right]\widehat{h} + \frac{1}{3}\widehat{h}^3 - \frac{1}{2}\widehat{h}^2\frac{d\widehat{\Gamma}}{dy} = \frac{1}{3}\beta\widehat{h}^3\frac{d\widehat{h}}{dy} - k_{\widehat{h},1}, \tag{3.13a}$$

$$-\left[\widehat{s}_1 + \eta_1 m'(t)\right]\widehat{\Gamma} + \frac{1}{2}\widehat{h}^2\widehat{\Gamma} - \widehat{h}\widehat{\Gamma}\frac{d\widehat{\Gamma}}{dy} = \frac{1}{2}\beta\widehat{h}^2\widehat{\Gamma}\frac{d\widehat{h}}{dy} + \delta\frac{d\widehat{\Gamma}}{dy} - k_{\widehat{\Gamma},1}, \tag{3.13b}$$

where the k's are constants and we have removed the assumption from (3.6) that the speed $\widehat{s}_1$ is known. Note that the $m'(t)$ terms are formally higher-order terms as $t \to \infty$, but we retain them in (3.13a) and (3.13b) to help indicate the fact that the boundary layer solution is slowly varying in time and has speed different from $x_0'(t)$ (see (3.12)). Neglecting this weak variation, observe that (3.13a) and (3.13b) take the same form as the traveling wave equations (2.2a) and (2.2b). Hence the boundary layer solution is also a traveling wave, see Figure 3.5. One difference, however, is that the solutions of (3.13a) and (3.13b) are subject to only the left boundary conditions $\widehat{h}(y \to -\infty) \to h_L$, $\widehat{\Gamma}(y \to -\infty) \to \Gamma_L$ which determine the constants of integration for $t \to \infty$ to be

$$k_{\widehat{h},1} = \widehat{s}_1 h_L - \frac{1}{3}h_L^3, \qquad k_{\widehat{\Gamma},1} = \widehat{s}_1\Gamma_L + \frac{1}{2}h_L^2\Gamma_L. \tag{3.13c}$$

In contrast to (2.3), note that the speed $\widehat{s}_1$ has not yet been determined.

An analogous set of boundary layer equations can be obtained in the neighborhood of η_2 with η_1 replaced by η_2 and different constants for $k_{\widehat{h},2}$ and $k_{\widehat{\Gamma},2}$, $\widehat{s}_2$ determined by the boundary conditions $\widehat{h}(y \to \infty) \to h_R$, $\widehat{\Gamma}(y \to \infty) \to 0$,

$$k_{\widehat{h},2} = \widehat{s}_2 h_R - \frac{1}{3}h_R^3, \qquad k_{\widehat{\Gamma},2} = 0. \tag{3.14}$$

The traveling wave structure of these solutions are shown in Figure 3.6. The need for this boundary layer is not as apparent as for (3.13a), (3.13b), and (3.13c) since the outer solution (3.10) is compatible with the boundary conditions for $y \to \infty$. However, like the solution at η_1, this solution at η_2 gives the structure defining the smooth transition from one level of h to another, $h_2 \to h_R$ ($h_L \to h_1$ at η_1), and from one slope of Γ to another, $\Gamma' = G_2 \to \Gamma' = 0$ ($\Gamma' = 0 \to \Gamma' = G_1$ at η_1).

With respect to system (3.3a) and (3.3b) the inner solutions exhibit sharpening features with the widths of the boundary layers decreasing as $t \to \infty$ (see insets in Figure 3.2). However, under the rescaling appropriate to the boundary layers, we observe

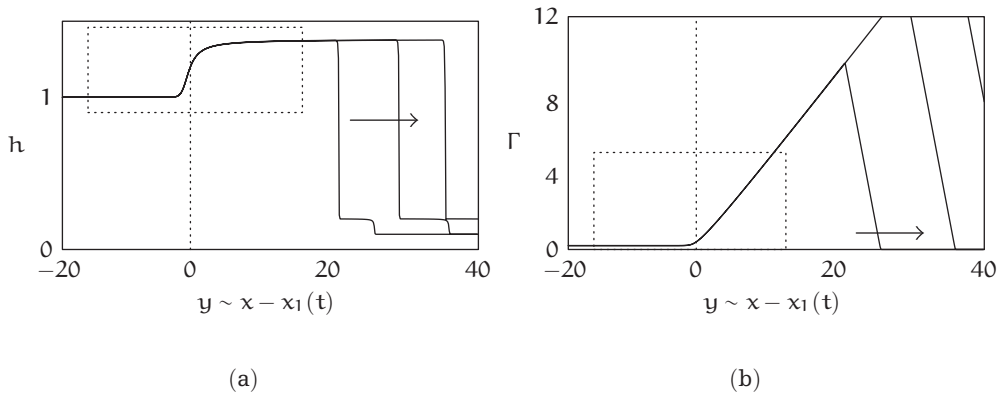

(a) (b)

Figure 3.5 The numerical solution profiles from Figure 3.2 shifted into the reference frame for the boundary layer at η_1, where locally (here roughly $y < 20$), the solution is a quasisteady traveling wave stationary in this frame (boxed). The outer solution spreads to the right in this reference frame.

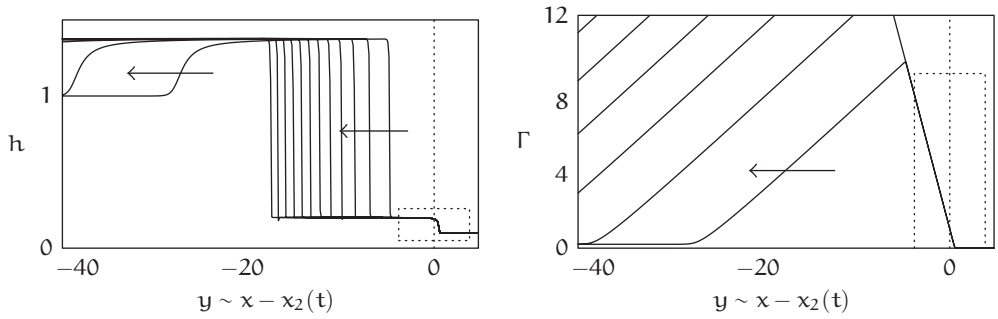

(a) (b)

Figure 3.6 The numerical solution profiles from Figure 3.2 shifted into the reference frame for the boundary layer at η_2, where locally (here roughly $-5 < y$), the solution is a quasisteady traveling wave stationary in this frame (boxed). The outer solution spreads to the left in this reference frame.

that these solutions are quasisteady traveling waves. Moreover, the boundary layer scaling essentially returns the system to the original form (1.1a) and (1.1b) with $y \sim x$, $\widehat{h} \sim h$, and $\widehat{\Gamma} \sim \Gamma$. Consequently, while for $\Gamma_L > 0$ the solution is not globally a traveling wave, traveling wave solutions still accurately describe h, Γ locally in these boundary layers (see Figures 3.5, 3.6).

3.3 Boundary layer at $\eta = 0$

As described above, on the $\zeta = O(1)$ lengthscale, for $m \to \infty$, the solution approaches (3.6) and appears to have jump discontinuities in $\widetilde{h}$, $\widetilde{\Gamma}'$ at $\zeta = 0$. Like the behavior at $\eta = \eta_1, \eta_2$, the presence of higher-order regularization smooths the solution over a narrow boundary layer at $\zeta = 0$. However, the structure at $\eta = 0$ is different than in the other boundary layers because here $\Gamma = O(m) \to \infty$ whereas $\Gamma = O(1)$ near η_1, η_2.

To characterize the boundary layer at $\eta = 0$, where Γ reaches its maximum, $m(t) = \Gamma_{max}(t)$, we use the ansatz

$$h(x,t) \sim \check{h}(\eta), \quad \Gamma(x,t) \sim m(t) + \check{\Gamma}(\eta), \quad \eta = x - st, \tag{3.15}$$

where $\check{h}, \check{\Gamma} = O(1)$ on $O(1)$ bounded neighborhoods of $\eta = 0$ as $m(t) \to \infty$. Note that $\check{\Gamma}(0) = 0$ from the definition of Γ_{max}. Substituting this ansatz into the original governing equations (1.1a) and (1.1b), the traveling wave equation (2.2a) for $\check{h}(\eta)$ is recovered at leading order from (1.1a),

$$-s\check{h} + \frac{1}{3}\check{h}^3 - \frac{1}{2}\check{h}^2\frac{d\check{\Gamma}}{d\eta} = \frac{1}{3}\beta\check{h}^3\frac{d\check{h}}{d\eta} - c_h. \tag{3.16a}$$

Substituting into (1.1b) and using (3.4) for $t \to \infty$, we obtain the dominant balance at $O(m)$,

$$\frac{1}{2}\check{h}^2 - \check{h}\frac{d\check{\Gamma}}{d\eta} = \frac{1}{3}\beta\check{h}^3\frac{d\check{h}}{d\eta} - c_\Gamma. \tag{3.16b}$$

Note that the influence of the regularization by surface diffusion, associated the parameter δ is not present in (3.16a) and (3.16b). On the other hand, the parameter $\beta > 0$ is essential in determining the structure of the boundary layer. In contrast, both β and δ were present in the (3.13a) and (3.13b) boundary layer equations.

Applying the boundary conditions at $\eta \to \pm\infty$ and using the result from [16] that

$$s = \frac{1}{6}\left(h_1^2 + h_1h_2 + h_2^2\right), \tag{3.17}$$

we obtain $c_\Gamma = -s$ and $c_h = h_1h_2(h_1 + h_2)/12 = k_h$, see (2.3). Consequently, (3.16a) and (3.16b) can be rewritten as the autonomous system

$$\frac{d\check{h}}{d\eta} = \frac{\left(\check{h} - h_1\right)\left(\check{h} - h_2\right)\left(\check{h} + h_1 + h_2\right)}{\beta\check{h}^3}, \qquad \frac{d\check{\Gamma}}{d\eta} = \frac{2s\left(\check{h} - h_*\right)}{\check{h}^2}, \tag{3.18}$$

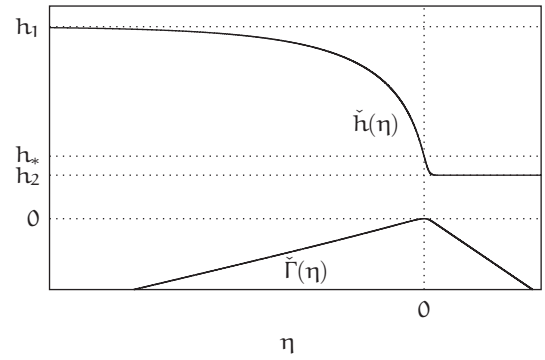

Figure 3.7 Structure of the boundary layer at $\eta = 0$ as described by (3.18).

where the constant h_* defines the film thickness at $\eta = 0$, $\check{h}(0) = h_*$, where $\check{\Gamma}(0) = 0$ ($\Gamma = \Gamma_{max}$),

$$h_* = \frac{3h_1h_2(h_1 + h_2)}{2(h_1^2 + h_1h_2 + h_2^2)}. \tag{3.19}$$

As expected, these equations describe a unique smooth solution connecting $h \to h_1$ to $h \to h_2$ and $\Gamma' \to G_1$ to $\Gamma' \to G_2$, see Figure 3.7.

3.4 Matching and overall structure

As $t \to \infty$ since the influence of quasistatic evolution becomes weak, it is valid to treat the outer solution (3.6) and the boundary layers as steady traveling waves to leading order. Consequently, the results of [16] may be applied directly to carry out the asymptotic matching of the boundary layers to the outer solution. Notably, it is found that the leading order wave speeds are identical,

$$s = \widehat{s}_1 = \widehat{s}_2 \tag{3.20}$$

for s given by (2.3). Briefly, matching the boundary layer at η_1 to the outer solution (3.10) requires finding a solution of (3.13a) and (3.13b) that satisfies $\widehat{h}(y \to \infty) \to h_1$ and $\widehat{\Gamma}(y \to \infty) \to \infty$ with $\widehat{\Gamma}'(y \to \infty) \to G_1$. Substituting these into (3.13b) yields $-\widehat{s}_1 + (1/2)h_1^2 - h_1G_1 = 0$, similar to [16]. It is notable that this algebraic matching condition, and likewise the one obtained from (3.13a) are independent of Γ_L. The consequence is that to leading order, despite the fact that the outer solution is a self-similar growing

profile (3.10), for long times the overall solution (outer and boundary layers) can be understood in terms of a single traveling wave with speed s.

4 Discussion and conclusions

The presence of a finite mass of insoluble surfactant on a film moving down an inclined substrate introduces new structure to the leading edge of the fluid film. Provided that the threshold condition (2.6) holds, despite the new structure of the film, the solution propagates with the same speed as if there were no surfactant.

When surfactant is continually supplied from upstream, the solution is no longer a traveling wave. While a well-defined wave speed is maintained, in the frame of reference moving with that speed, the solution exhibits a self-similar growing form for $t \to \infty$; similar behavior has been observed in other thin film problems [8, 24]. We have been able to obtain expressions for the accumulation of surfactant and leading order asymptotic forms for the film and surfactant profiles subject to relatively few assumptions on the dynamics. While the arguments presented here are not rigorous, the approaches considered could provide good starting points for further analyses of this problem.

In forthcoming work [17], further analysis of the traveling wave (2.4) will be presented: structural stability with respect to regularization and the limits of $\beta \to 0$, $\delta \to 0$ and weak fourth-order capillary effects, as well as other questions of stability. It is worth noting again that the solutions presented here depend on the threshold condition (2.6). Above this threshold, for example in the case of an initially flat film, the form of solutions is not known, and numerical simulations suggest that more complicated dynamics take place [16]. Further work on this problem is being pursued [17].

Acknowledgments

We thank the referee for incisive questions and helpful suggestions that improved the article. Parts of this research were presented by MS at the IPAM workshop on thin films and fluid interfaces. We thank the organizers and IPAM for an enjoyable and productive meeting. The first and third authors were supported by NSF Grants DMS-0239125 CAREER and DMS-0244498 FRG. The second author was supported by NSF Grant DMS-0244491 FRG.

References

[1] A. L. Bertozzi, *The mathematics of moving contact lines in thin liquid films*, Notices of the American Mathematical Society **45** (1998), no. 6, 689–697.

[2] A. L. Bertozzi, A. Münch, and M. Shearer, *Undercompressive shocks in thin film flows*, Physica D: Nonlinear Phenomena **134** (1999), no. 4, 431–464.

[3] M. S. Borgas and J. B. Grotberg, *Monolayer flow on a thin film*, Journal of Fluid Mechanics **193** (1988), 151–170.

[4] J. Buckmaster, *Viscous sheets advancing over dry beds*, Journal of Fluid Mechanics **81** (1977), no. 4, 735–756.

[5] A. D. Dussaud, O. K. Matar, and S. M. Troian, *Spreading characteristics of an insoluble surfactant film on a thin liquid layer: comparison between theory and experiment*, Journal of Fluid Mechanics **544** (2005), 23–51.

[6] B. D. Edmonstone, O. K. Matar, and R. V. Craster, *Flow of surfactant-laden thin films down an inclined plane*, Journal of Engineering Mathematics **50** (2004), no. 2-3, 141–156.

[7] ———, *Surfactant-induced fingering phenomena in thin film flow down an inclined plane*, Physica D: Nonlinear Phenomena **209** (2005), no. 1–4, 62–79.

[8] J. C. Flitton and J. R. King, *Surface-tension-driven dewetting of Newtonian and power-law fluids*, Journal of Engineering Mathematics **50** (2004), no. 2-3, 241–266.

[9] H. Garcke and S. Wieland, *Surfactant spreading on thin viscous films: nonnegative solutions of a coupled degenerate system*, SIAM Journal on Mathematical Analysis **37** (2006), no. 6, 2025–2048.

[10] B. H. Gilding and R. Kersner, *Travelling Waves in Nonlinear Diffusion-Convection Reaction*, Progress in Nonlinear Differential Equations and Their Applications, vol. 60, Birkhäuser, Basel, 2004.

[11] M. H. Holmes, *Introduction to Perturbation Methods*, Texts in Applied Mathematics, vol. 20, Springer, New York, 1995.

[12] H. Huppert, *Flow and instability of a viscous current down a slope*, Nature **300** (1982), no. 5891, 427–429.

[13] O. E. Jensen and J. B. Grotberg, *Insoluble surfactant spreading on a thin viscous film: shock evolution and film rupture*, Journal of Fluid Mechanics **240** (1992), 259–288.

[14] ———, *The spreading of heat or soluble surfactant along a thin liquid film.*, Physics of Fluids A **5** (1993), no. 1, 58–68.

[15] J. Kevorkian and J. D. Cole, *Multiple Scale and Singular Perturbation Methods*, Applied Mathematical Sciences, vol. 114, Springer, New York, 1996.

[16] R. Levy and M. Shearer, *The motion of a thin film driven by surfactant and gravity*, SIAM Journal of Applied Mathematics **66** (2006), no. 5, 1588–1609.

[17] R. Levy, M. Shearer, and T. P. Witelski, *Traveling waves in thin liquid films driven by gravity and a finite volume of surfactant*, in preparation.

[18] J. D. Logan, *Transport Modeling in Hydrogeochemical Systems*, Interdisciplinary Applied Mathematics, vol. 15, Springer, New York, 2001.

[19] H.-W. Lu, K. Glasner, A. L. Bertozzi, and C.-J. Kim, *A diffuse interface model for electrowetting droplets in a Hele-Shaw cell*, submitted to Journal of Fluid Mechanics.

[20] O. K. Matar and S. M. Troian, *Growth of non-modal transient structures during the spreading of surfactant coated films*, Physics of Fluids **10** (1998), no. 5, 1234–1236.

[21] ———, *The development of transient fingering patterns during the spreading of surfactant coated films*, Physics of Fluids **11** (1999), no. 11, 3232–3246.

[22] J. A. Moriarty, L. W. Schwartz, and E. O. Tuck, *Unsteady spreading of thin liquid films with small surface tension*, Physics of Fluids A **3** (1991), no. 5, 733–742.

[23] A. Münch, *Pinch-off transition in Marangoni-driven thin films*, Physical Review Letters **91** (2003), Article ID 016105, no. 1.

[24] A. Münch, B. Wagner, and T. P. Witelski, *Lubrication models with small to large slip lengths*, Journal of Engineering Mathematics **53** (2005), no. 3-4, 359–383.

[25] T. G. Myers, *Thin films with high surface tension*, SIAM Review **40** (1998), no. 3, 441–462.

[26] A. Oron, S. H. Davis, and S. G. Bankoff, *Long-scale evolution of thin liquid films*, Reviews of Modern Physics **69** (1997), no. 3, 931–980.

[27] M. Renardy, *A singularly perturbed problem related to surfactant spreading on thin films*, Nonlinear Analysis. Theory, Methods & Applications **27** (1996), no. 3, 287–296.

[28] ———, *On an equation describing the spreading of surfactants on thin films*, Nonlinear Analysis. Theory, Methods & Applications **26** (1996), no. 7, 1207–1219.

[29] ———, *A degenerate parabolic-hyperbolic system modeling the spreading of surfactants*, SIAM Journal on Mathematical Analysis **28** (1997), no. 5, 1048–1063.

[30] L. W. Schwartz and R. V. Roy, *Theoretical and numerical results for spin coating of viscous liquids*, Physics of Fluids **16** (2004), no. 3, 569–584.

[31] E. O. Tuck and L. W. Schwartz, *A numerical and asymptotic study of some third-order ordinary differential equations relevant to draining and coating flows*, SIAM Review **32** (1990), no. 3, 453–469.

[32] A. I. Volpert, V. A. Volpert, and V. A. Volpert, *Traveling Wave Solutions of Parabolic Systems*, Translations of Mathematical Monographs, vol. 140, American Mathematical Society, Rhode Island, 1994.

Thomas P. Witelski: Department of Mathematics and Center for Nonlinear and Complex Systems, Duke University, Durham, NC 27708-0320, USA
E-mail address: witelski@math.duke.edu

Michael Shearer: Department of Mathematics and Center for Research in Scientific Computation, N.C. State University, Raleigh, NC 27695, USA
E-mail address: shearer@ncsu.edu

Rachel Levy: Department of Mathematics, Duke University, Durham, NC 27708-0320, USA; Department of Mathematics, Harvey Mudd College, 1250 N. Dartmouth Avenue, Claremont, CA 91711, USA
E-mail address: levy@hmc.edu